Engineering Analysis with Boundary Elements 34 (2010) 785–792

Contents lists available at ScienceDirect

Engineering Analysis with Boundary Elements

journal homepage: www.elsevier.com/locate/enganabound

A meshless method based on RBFs method for nonhomogeneous backward heat conduction problem

Ming Li [a], Tongsong Jiang [b,c,*], Y.C. Hon [a]

[a] Department of Mathematics, City University of Hong Kong, Hong Kong SAR, China
[b] Department of Mathematics, Linyi Normal University, Shandong, China
[c] College of Computer Science and Technology, Shandong University, Jinan, China

ARTICLE INFO

Article history:
Received 2 November 2009
Accepted 19 March 2010
Available online 11 May 2010

Keywords:
RBF
Meshless methods
BHCP
Ill-posed problem

ABSTRACT

Based on the idea of radial basis functions approximation and the method of particular solutions, we develop in this paper a new meshless computational method to solve nonhomogeneous backward heat conduction problem. To illustrate the effectiveness and accuracy of the proposed method, we solve several benchmark problems in both two- and three-dimensions. Numerical results indicate that this novel approach can achieve an efficient and accurate solution even when the final temperature data is almost undetectable or disturbed with large noises. It has also been shown that the proposed method is stable to recover the unknown initial temperature from scattered final temperature data.

1. Introduction

In this paper we develop a new computational method for solving nonhomogeneous backward heat conduction problem (NBHCP). Backward heat conduction problem (BHCP) arises in the modeling of heat propagation in thermophysics and mechanics of continuous media. The determination of the unknown initial temperature from observable scattered final temperature data is required in many real applications. The solution process for BHCP, however, is in nature “unstable” because the unknown solutions/parameters have to be determined from indirect observable data which contain measurement error. The major difficulty in establishing any numerical algorithm for approximating the solution is due to the severe ill-posedness of the problem and the ill-conditioning of the resultant discretized matrix. Another difficulty to establish any numerical solution for the BHCP is due to the nature of its physical phenomena. Although heat conduction process is very smooth, the process is irreversible. In other words, the characteristic of the solution (for instance, the shape of the interior heat flow) is not affected by the observed data.

BHCP is typically ill-posed in the sense of Hadamard [10] which means that any small error in the collected data may induce enormous error to the solution. In general, the solution of BHCP does not exist and even if it exists it is not continuously dependent on the final data, see Payne [31]. Uniqueness conditions for the BHCP have been investigated by Miranker [30].

Numerical methods for the ill-posed BHCP have been given in the works of boundary element method (BEM) [11], finite difference method (FDM) [28,32], perturbation technique [25], iterative boundary element method [24,27], mollification method [18], method of fundamental solutions (MFS) [19–21,29], Tikhonov regularization [7] and quasi-boundary regularization [2] techniques. Most of these methods are developed for solving homogeneous BHCP or problems in one-dimensional spatial domain. For instances, the MFS cannot be extended to solve nonhomogeneous partial differential equations (PDEs) whereas the BEM, FDM and mollification method are difficult to solve BHCPs in higher dimensional space.

Recently, meshless methods based on radial basis functions (RBFs) have been developed to solve various inverse problems [4,35]. In comparing with the mesh dependent methods (FDM, BEM, and finite element method (FEM)) [8], the meshless methods have the following advantages:

- They can be applicable to solve more general class of problems defined on irregular domains.
- They are readily extendable to solve high-dimensional problems.

In this paper we propose a new computational method to deal with NBHCP in two- or three-dimensional spatial domains. The main idea is to first reduce the nonhomogeneous heat conduction equation into a series of elliptic PDEs by using the method of lines. Each elliptic PDE is then converted into an equivalent standard Poisson equation whose solution can be obtained by using the RBFs as particular solutions. To tackle the ill-conditioning

* Corresponding author.
E-mail addresses: liming04@gmail.com (M. Li), tsjemail@163.com (T. Jiang).

0955-7997/$ - see front matter © 2010 Elsevier Ltd. All rights reserved.
doi:10.1016/j.enganabound.2010.03.010

problem of the resultant system of linear equations, we adapt the use of the standard Tikhonov regularization technique with L-curve method [15–17] for choosing the optimal regularized parameter.

The structure of the paper is organized as follows: In Section 2, we first transform the original nonhomogeneous parabolic PDE into a series of elliptic PDEs. Based on the idea of RBFs and the use of particular solutions, we then give an approximation to the solution of each elliptic PDE. In Section 3, the efficiency and accuracy of the proposed method are verified by solving several NBHCPs in two- and three-dimensional spatial domains. Numerical examples are also given to illustrate the stability of the proposed method.

2. Methodology

Let $u(\mathbf{x},t)$ satisfy the following heat conduction equation:

$$\frac{\partial}{\partial t}u(\mathbf{x},t)+f(\mathbf{x},t)=\Delta u(\mathbf{x},t), \quad (\mathbf{x},t)\in \Omega\times(0,T); \tag{1}$$

under the final temperature condition

$$u(\mathbf{x},T)=g(\mathbf{x}), \quad \mathbf{x}\in\Omega; \tag{2}$$

and the Dirichlet boundary condition

$$u(\mathbf{x},t)=h(\mathbf{x},t), \quad \mathbf{x}\in\Gamma,\ 0<t<T; \tag{3}$$

where $f(\mathbf{x},t)$, $g(\mathbf{x})$, $h(\mathbf{x},t)$ are known functions, $\Omega\subset\mathbb{R}^d, d=2,3$ is a connected and bounded domain and $\Gamma=\partial\Omega$ is the boundary of the domain Ω.

In practical application, the final temperature condition (2) and the Dirichlet boundary condition (3) are given only at some discrete points, say, $(\mathbf{x}_i,T)$, $i=1,\dots,n_I$ on $\Omega\times\{T\}$ which satisfy the final condition (2) and $(\mathbf{x}_i,t_i)$, $i=n_I+1,\dots,n_I+n_B$ on $\Gamma\times\ (0,T)$ which satisfy the boundary condition (3). The NBHCP to be investigated in this paper is then to determine the unknown initial temperature $u(\mathbf{x},0)$ from the given discrete data.

To illustrate how to apply the RBFs and particular solutions as a spatial meshless collocation scheme to solve the NBHCP, we first reduce the above nonhomogeneous parabolic PDE into a series of elliptic PDEs using the method of lines in the following section. We note here that there are other reduction techniques such as Laplace transform and Fourier transform that can achieve the same purpose.

Let $\delta t=T/n_T$ be the time step size and $t^l=l\delta t$, $l=0,\dots,n_T$ denote the discretization of the time interval $(0,T]$. For any $t\in[t^l,t^{l+1})$, we approximate $u(\mathbf{x},t)$ and $\partial u(\mathbf{x},t)/\partial t$ by:

$$u(\mathbf{x},t)\backsimeq u(\mathbf{x},t^l), \tag{4}$$

and

$$\frac{\partial u(\mathbf{x},t)}{\partial t}\backsimeq\frac{u(\mathbf{x},t^{l+1})-u(\mathbf{x},t^l)}{\delta t}, \tag{5}$$

respectively.

For simplicity, we denote $u^l(\mathbf{x})\equiv u(\mathbf{x},t^l)$, $h^l(\mathbf{x})\equiv h(\mathbf{x},t^l)$ and $f^l(\mathbf{x})\equiv f(\mathbf{x},t^l)$. Substituting (4) and (5) into Eqs. (1)–(3), we obtain the following series of elliptic PDEs:

$$\frac{u^{l+1}(\mathbf{x})-u^l(\mathbf{x})}{\delta t}=\Delta u^l(\mathbf{x})-f^l(\mathbf{x}), \tag{6}$$

where $l=0,\dots,(n_T-1)$. Each of these elliptic PDEs will be solved iteratively starting from the final condition (2) which gives $u^{n_T}(\mathbf{x})=g(\mathbf{x})$. Eq. (6) can be rewritten as

$$\Delta u^l(\mathbf{x})+\frac{1}{\delta t}u^l(\mathbf{x})=f^l(\mathbf{x})+\frac{1}{\delta t}u^{l+1}(\mathbf{x}). \tag{7}$$

From Eq. (7) it can be seen that the original NBHCP has been reduced to a series of nonhomogeneous elliptic PDEs in which each of these elliptic PDEs is in fact a Helmholtz equation. It is well known that the ill-conditionedness of solving the Helmholtz equation increases as the coefficient $1/\delta t$ increases. Therefore, the step size δt cannot be too small for obtaining stable solution. This restriction on the time step size will be verified in the next section on numerical examples.

To obtain a solution to each of the elliptic PDEs (7) under boundary condition:

$$u^l(\mathbf{x})=h^l(\mathbf{x}), \tag{8}$$

we first rewrite (7) as

$$\Delta u^l(\mathbf{x})=f^l(\mathbf{x})+\frac{1}{\delta t}u^{l+1}(\mathbf{x})-\frac{1}{\delta t}u^l(\mathbf{x}). \tag{9}$$

By expressing the right-hand side of Eq. (9) as a function with respect to $\mathbf{x}$, we obtain the following standard Poisson-type equations: For each $l=0,\dots,(n_T-1)$,

$$\Delta u^l(\mathbf{x})=F^l(\mathbf{x}). \tag{10}$$

If the fictitious function $F^l(\mathbf{x})$ is known, then Eq. (1) is equivalent to the Poisson-type Eq. (10) under the same boundary condition.

Based on the idea of RBFs method, we approximate the function $F^l(\mathbf{x})$ by RBFs $\{\phi_j\}_{j=1}^n$ as:

$$F^l(\mathbf{x})\simeq\sum_{j=1}^n\alpha_j^l\phi_j(\mathbf{x}), \tag{11}$$

where $n=n_I+n_B$. From Eq. (10), each of the solutions $u^l(\mathbf{x})$ can then be approximated by

$$u^l(\mathbf{x})\simeq\sum_{j=1}^n\alpha_j^l\Phi_j(\mathbf{x}), \tag{12}$$

where Φ is called particular solution obtained by analytically solving

$$\Delta\Phi(\mathbf{x})=\phi(\mathbf{x}). \tag{13}$$

If we choose ϕ to be the multiquadric basis function (MQ), $\phi=\sqrt{r^2+c^2}$, $r=\|\mathbf{x}-\bullet\|$, $\mathbf{x}\in\mathbb{R}^d$, $d=2,3$, then the particular solution Φ is given by:

$$\Phi(r)=\begin{cases}\frac{1}{9}(4c^2+r^2)\sqrt{r^2+c^2}-\frac{c^3}{3}\ln(c+\sqrt{r^2+c^2}), & d=2,\\ \begin{cases}\frac{c^3}{3}, & r=0\\ \frac{(5c^2+2r^2)\sqrt{r^2+c^2}}{24}+\frac{c^4}{8r^2}\ln\left(\frac{r^2+\sqrt{r^2+c^2}}{c}\right), & r>0,\end{cases} & d=3,\end{cases} \tag{14}$$

where c is called the shape parameter of MQ. It is well known that the value of c is crucial to the exponential convergence property of using MQ for solving partial differential equations. Formula for an optimal shape parameter c by reducing residual errors has recently been given by Huang et al. [22]. For numerical verification of the proposed method, we simply use MQ with constant $c=1$ in all of the numerical computations given in this paper. Other radial basis functions ϕ, such as smoothing spline r^{2m-1} that does not contain a shape parameter, can also be chosen and their corresponding Φ can be derived similarly. Denote

$$\phi_j(\mathbf{x})=\sqrt{r_j^2+c^2}, \tag{15}$$

where $r_j=\|\mathbf{x}-\mathbf{x}_j\|$, $\mathbf{x}\in\mathbb{R}^d$, $d=2,3$. We then have $\Delta\Phi_j(\mathbf{x})=\phi_j(\mathbf{x})$ for each $1\le j\le n$.

Since the fictitious function $F^l(\mathbf{x})$ is unknown at each time step l, we substitute the unknown solution $u^l(\mathbf{x})=\sum_{j=1}^n\alpha_j^l\Phi_j(\mathbf{x})$ into

Eqs. (7) and (8) to obtain: For each $l=0,\ldots,(n_T-1)$,

$$\sum_{j=1}^{n} \alpha_j^l \left(\phi_j(\mathbf{x}) + \frac{1}{\delta t} \Phi_j(\mathbf{x}) \right) = f^l(\mathbf{x}) + \frac{1}{\delta t} u^{l+1}(\mathbf{x}), \quad \mathbf{x} \in \Omega, \tag{16}$$

$$\sum_{j=1}^{n} \alpha_j^l \Phi_j(\mathbf{x}) = h^l(\mathbf{x}), \quad \mathbf{x} \in \Gamma. \tag{17}$$

For numerical verification of the proposed method in the next section, we uniformly choose n_I collocation points $\{\mathbf{x}_i\}_{i=1}^{n_I}$ in the interior of domain Ω and n_B collocation points $\{\mathbf{x}_i\}_{i=n_I+1}^{n_B}$ on the boundary Γ, where $n=n_I+n_B$. At each time level t^l, we need to solve the following system of linear equations for the undetermined coefficients α_j^l:

$$\sum_{j=1}^{n} \alpha_j^l \left(\phi_j(\mathbf{x}_i) + \frac{1}{\delta t} \Phi_j(\mathbf{x}_i) \right) = G^l(\mathbf{x}_i), \quad i=1,\ldots,n_I, \tag{18}$$

$$\sum_{j=1}^{n} \alpha_j^l \Phi_j(\mathbf{x}_i) = h^l(\mathbf{x}_i), \quad i=n_I+1,\ldots,n, \tag{19}$$

where $G^l(\mathbf{x}_i)=f^l(\mathbf{x}_i)+(1/\delta t)u^{l+1}(\mathbf{x}_i)$.

In matrix form, the values of the unknown coefficients $\alpha^l=(\alpha_1^l\alpha_2^l,\ldots,\alpha_n^l)^{tr}$ can be obtained from solving the following matrix equation:

$$A\alpha^l = b^l, \tag{20}$$

where A is a $n \times n$ coefficient matrix

$$A = \begin{pmatrix} \phi_j(\mathbf{x}_i)+\frac{1}{\delta t}\Phi_j(\mathbf{x}_i) \\ \Phi_j(\mathbf{x}_k) \end{pmatrix}_{n\times n},$$

here, $j=1,\ldots,n$, $i=1,\ldots,n_I$, $k=n_I+1,\ldots,n$ and b^l is the $n\times 1$ vector:

$$b^l = (G^l(x_1),\ldots,G^l(x_{n_I}),h^l(x_{n_I+1}),\ldots,h^l(x_n)).$$

Since the original problem (1)–(3) is highly ill-posed, the ill-conditioning of the matrix A in Eq. (20) still persists. In other words, most standard numerical methods cannot achieve good accuracy in solving the matrix Eq. (20) due to the bad conditioning of the matrix A. In fact, the condition number of the matrix A increases dramatically with respect to the total number of collocation points. Several regularization methods have been developed for solving these kinds of ill-conditioning problems [15–17]. In our computation we adapt the Tikhonov regularization technique [34] to solve the matrix Eq. (20). The Tikhonov regularized solution α_λ for Eq. (20) is defined to be the solution to the following penalized least square problem:

$$\min_{\alpha^l}\{\|A\alpha^l-b^l\|^2+\lambda^2\|\alpha^l\|^2\}, \tag{21}$$

where λ is called the regularization parameter.

The determination of a suitable value of the regularization parameter λ is crucial and is still under intensive research (refer [33,34]). In our computation we use the L-curve method, which is a kind of noise-free rule, to determine a suitable value of λ. The L-curve method was firstly developed by Lawson and Hanson [26] and applied by Chen et al. [3] for solving deconvolution problem. Hansen and O'Leary [17] investigated the properties of regularized systems under different values of the regularization parameter λ. The L-curve method is sketched in the following:

Define a curve

$$L=\{(\log(\|\alpha_\lambda\|^2), \quad \log(\|A\alpha_\lambda-b\|^2)),\lambda>0\}. \tag{22}$$

The curve is known as L-curve and a suitable regularization parameter λ is one that corresponds to a regularized solution near the "corner" of the L-curve [13–15].

In our computation, we used the Matlab code developed by Hansen [16] for solving the discrete ill-conditioned system (20). Denote the regularized solution of (20) by α^{λ^*} with the parameter λ^* chosen by above L-curve method when $l=n_T-1$. The approximate solution $\tilde{u}_{\lambda^*}(x,0)$ for the problem (1)–(3) is then given as

$$\tilde{u}_{\lambda^*}(x,0) = \sum_{j=1}^{n} \alpha_j^{\lambda^*}\Phi_j(x). \tag{23}$$

3. Numerical verification

The maximum error (Maxerror) and the root-mean-square error (RMSE) are used in the computations to compare the accuracy of the approximated solutions with the exact solutions. The Maxerror and RMSE are defined as follows:

$$Maxerror = \max_{1\le j\le N}|\tilde{u}_j-u_j|, \quad RMSE=\sqrt{\frac{1}{N}\sum_{j=1}^{N}(\tilde{u}_j-u_j)^2},$$

where N is the total number of testing nodes chosen randomly within the domain $\overline{\Omega}$ and $\hat{u}_j$ denotes the approximate solution at the jth node.

To demonstrate the effectiveness and stability of the meshless computation method proposed in the last section, several examples for solving the NBHCPs in both 2D and 3D are presented in the following subsections. Throughout this section, the noisy data in interior collocation points and boundary collocation points are generated by

$$\tilde{b} = b(1+\text{randn}\times\delta), \tag{24}$$

where b denotes the exact right-hand side of Eq. (20), δ is the tolerated noise level and *randn* is Gaussian random number with mean 0 and variance 1.

3.1. Numerical example for two-dimensional NBHCP

Example 1. Consider the following nonhomogeneous two-dimensional backward heat conduction equation:

$$\frac{\partial}{\partial t}u(\mathbf{x},t)+f(\mathbf{x},t)=\Delta u(\mathbf{x},t), \quad (\mathbf{x},t)\in\Omega\times(0,T)\subset\mathbb{R}^2\times\mathbb{R}^+, \quad \mathbf{x}=(x,y), \tag{25}$$

with final condition

$$u(\mathbf{x},T)=(y\sin(\pi x)+x\cos(\pi y))\cos(T), \quad \mathbf{x}\in\Omega, \tag{26}$$

and the measured Dirichlet boundary condition

$$u(\mathbf{x},t)=(y\sin(\pi x)+x\cos(\pi y))\cos(t), \quad \mathbf{x}\in\partial\Omega, \quad t>0, \tag{27}$$

where

$$f(\mathbf{x},t)=-\pi^2(y\sin(\pi x)+x\cos(\pi y))\cos(t)+(y\sin(\pi x)+x\cos(\pi y))\sin(t),$$

and the analytical solution given as:

$$u(\mathbf{x},t)=(y\sin(\pi x)+x\cos(\pi y))\cos(t). \tag{28}$$

We first consider the domain Ω to be the unit circle:

$$\Omega=\{(x,y): x=\cos\theta, y=\sin\theta, -\pi\le\theta\le\pi\}$$

as illustrated in Fig. 1.

In the computation, we choose $n_I=69$, $n_B=20$, $\delta t=0.25$, $c=1$ and $N=137$. The proposed method given in the previous section is then applied to obtain an approximation to the solution. Fig. 1 gives the RMSE for different noise level δ. Fig. 2 displays the numerical solution $\tilde{u}$ and the absolute difference between the exact solution and the numerical solution for $T=1$ and $\delta=10E-3$.

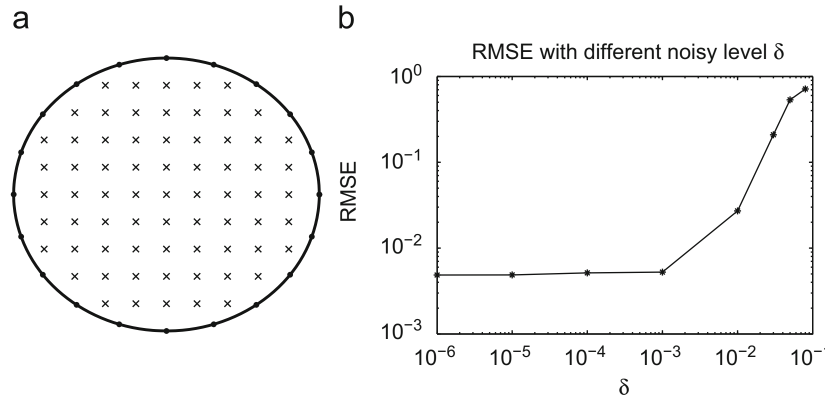

Fig. 1. The left figure displays the domain as the unit circle with boundary collocation points (•) and interior collocation points (×). The right figure gives the RMSE with different noise level δ for $T=1$ and $\delta t=0.25$.

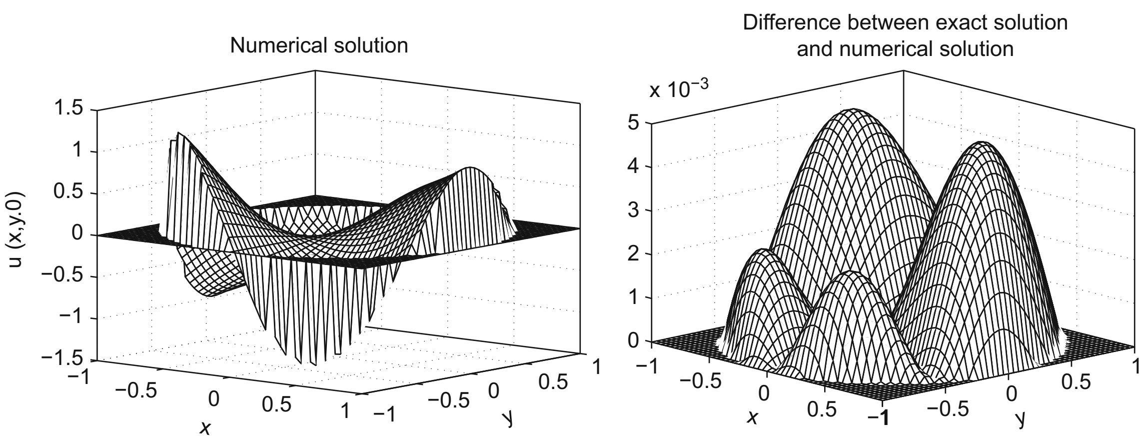

Fig. 2. The left figure displays the numerical solution $\tilde{u}$ and the right figure shows the absolute difference between the exact solution and the numerical solution for $T=1$ and $\delta=10E-3$.

Table 1
Maxerror and RMSE with different time steps δt and final time T.

	$\delta t=1$	$\delta t=1/2$	$\delta t=1/3$	$\delta t=1/4$
$T=1$				
Maxerror	1.910E−02	9.759E−03	6.839E−03	5.256E−03
RMSE	5.360E−03	3.028E−03	2.1928E−03	1.722E−03
$T=2$				
Maxerror	2.853E−02	1.897E−02	1.336E−02	1.001E−02
RMSE	7.953E−03	4.493E−03	3.194E−03	2.454E−03
$T=3$				
Maxerror	2.681E−02	2.563E−02	1.868E−02	1.470E−02
RMSE	7.476E−03	6.435E−03	4.752E−03	3.789E−03

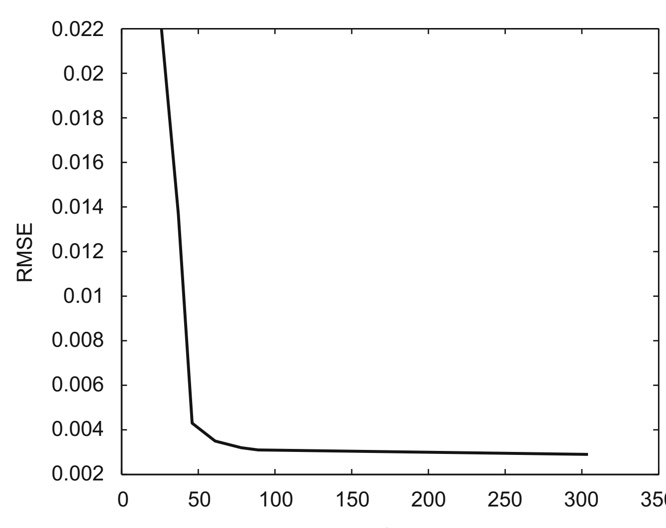

Fig. 3. The RMSE with various values of n.

In addition, the Maxerror and RMSE for $T=1,2,3$ are shown in Table 1 using various time steps $\delta t=1,1/2,1/3,1/4$ with noise level $\delta=10E-3$. It can be seen from Figs. 1 and 2 and Table 1 that the proposed method performs well for solving the two-dimensional NBHCP (Fig. 3).

For further investigations, the convergence of the numerical solution with increasing $n=n_I+n_B$ are shown in Fig. 4. Here, we choose $T=2$, $\delta t=1/4$ and noise level $\delta=10E-3$. It can be seen that the numerical solution converges very fast with increasing n. Hence, small n is used in following examples. At the same time, the regularization parameters λ for different t are shown in Table 2 with other parameters $T=2$, $\delta t=1/4$, $n_I=69$ and $n_B=20$.

Example 2. In this example, we consider the same exact u and the same equation given in Example 1 but with a different domain defined as the region enclosed by the Cassini curve obtained from

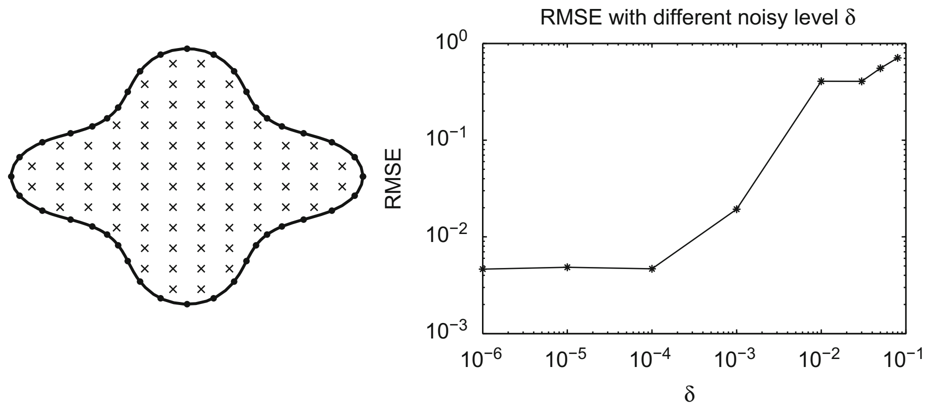

Fig. 4. The left figure display the domain enclosed by the Cassini curve, the boundary collocation points (•) and the interior collocation points (×). The right figure plots the RMSE with different noise level δ for $T=1$ and $\delta t=1/5$.

Table 2
The regularization parameter λ with respect to different t when $T=2$ and $\delta=1/4$.

t	0	1	2	3	4	5	6	7
λ^*	3.328E−09	3.328E−09	3.328E−09	3.513E−09	3.513E−09	3.328E−09	7.507E−09	5.135E−09

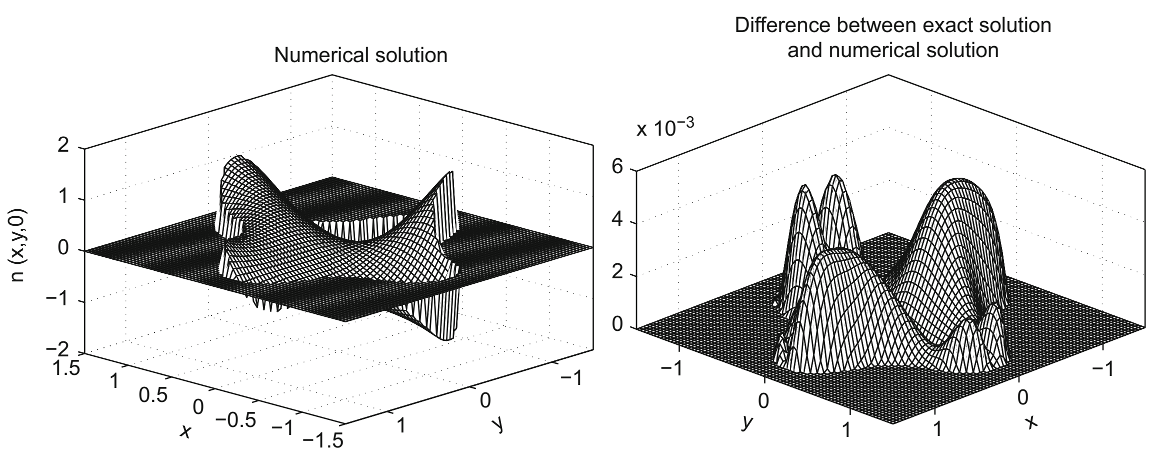

Fig. 5. The left figure displays the numerical solution and the right figure plots the absolute difference between the exact solution and the numerical solution for $T=1$ and $\delta=10E{-}3$.

Table 3
Maxerror and RMSE with different time steps δt and final time T.

	$\delta t=1$	$\delta t=1/2$	$\delta t=1/3$	$\delta t=1/4$	$\delta t=1/5$
$T=1$					
Maxerror	2.007E−02	1.021E−02	6.895E−03	5.152E−03	4.573E−03
RMSE	4.555E−03	2.536E−03	1.770E−03	1.369E−03	1.124E−03
$T=2$					
Maxerror	1.975E−02	1.021E−02	6.866E−03	5.439E−03	2.944E−01
RMSE	3.788E−03	2.035E−03	1.394E−03	1.063E−03	3.108E−02
$T=3$					
Maxerror	1.978E−02	1.031E−02	7.752E−03	6.462E−03	1.501E+02
RMSE	4.060E−03	2.207E−03	1.515E−03	1.177E−03	1.313E+01

the parametric equation:

$$\partial\Omega = \{(x,y) : x = \rho\cos\theta, y = \rho\sin\theta, -\pi \le \theta \le \pi\}, \tag{29}$$

where

$$\rho = (\cos(4\theta) + \sqrt{2 - \sin^2(4\theta)})^{1/4}. \tag{30}$$

In this computation, we choose $n_I=37$, $n_B=40$, $\delta t = 1/5$, $c=1$ and $N=74$. Fig. 4 displays the domain and gives the RMSE with different noise level δ with final time $T=1$. The numerical solution and the absolute difference between the exact solution and the numerical solution for $T=1$ and $\delta t = 1/5$ are plotted in Fig. 5. In addition, the Maxerror and RMSE for $T=1,2,3$ are shown in Table 3 using various time steps $\delta t = 1, 1/2, 1/3, 1/4, 1/5$. It can again be seen from Fig. 5 and Table 3 that the proposed method performs well when the time step sizes are $\delta t = 1/3, 1/4$. Besides, it is observed that the Maxerror and RMSE do not decrease as the time step δt decreases due to the reason we mentioned in Section 2.

Example 3. To further explore the application of the proposed method for solving two-dimensional NBHCPs, we consider the following severe example:

$$\frac{\partial}{\partial t} u(\mathbf{x},t) + f(\mathbf{x},t) = \Delta u(\mathbf{x},t), \quad (\mathbf{x},t) \in \Omega \times (0,T) \subset \mathbb{R}^2 \times \mathbb{R}^+, \quad \mathbf{x} = (x,y), \tag{31}$$

with final condition

$$u(\mathbf{x},T) = \sin(\pi(x+y))e^{-\pi^2 T}, \quad \mathbf{x} \in \Omega, \tag{32}$$

and measured Dirichlet boundary condition

$$u(\mathbf{x},t) = \sin(\pi(x+y))e^{-\pi^2 t}, \quad \mathbf{x} \in \partial\Omega, \ t > 0, \tag{33}$$

where $f(\mathbf{x},t) = 0$ and the analytical solution given as follows:

$$u(\mathbf{x},t) = \sin(\pi(x+y))e^{-\pi^2 t}. \tag{34}$$

The case when the domain is the unit square domain $[0,1] \times [0,1]$ is a typical benchmark example for testing the efficiency and accuracy of any numerical method for solving two-dimensional BHCP.

In this example, we choose $n_I=81$, $n_B=40$, $\delta t = 0.1$, $c=1$ and $N=361$. Fig. 6 displays the domain Ω and the RMSE with different noise level δ with the final time $T=1$. Fig. 7 displays the numerical solution and its absolute difference between the exact solution for $T=1$ and $n_T=15$. In addition, the Maxerror and RMSE for $T=1,2,3$ are shown in Table 4. It can be seen that the proposed method also performs well in this benchmark problem.

3.2. Numerical example for three-dimensional NBHCP

In this subsection, it will be shown that the proposed method is also applicable to solve three-dimensional NBHCP.

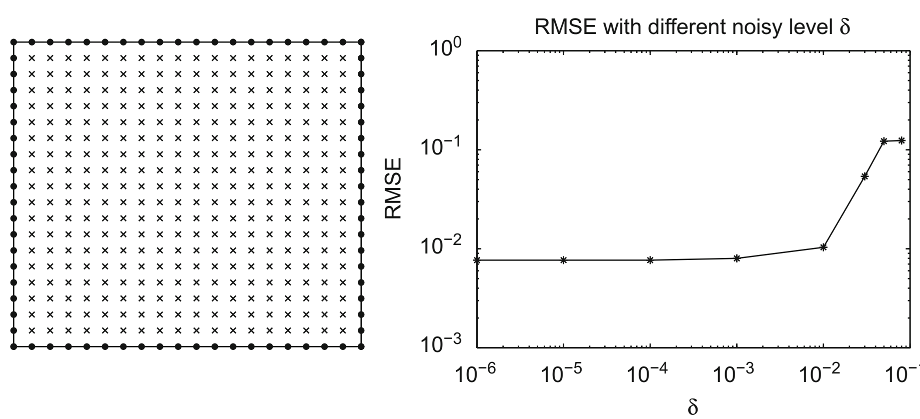

Fig. 6. The left figure displays the unit square domain, boundary collocation points (•) and interior boundary points (×). The right figure shows the RMSE with different noise level δ for $T=1$ and $\delta t = 0.1$.

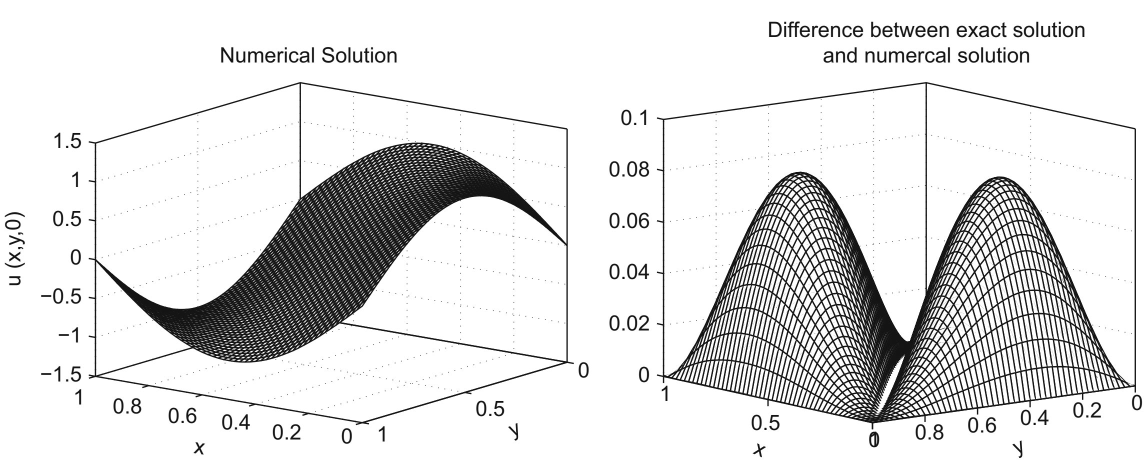

Fig. 7. The left figure displays the numerical solution and the right figure shows the absolute difference between the exact solution and the numerical solution for $T=1$ and $\delta = 10E-3$.

Table 4
Maxerror and RMSE with different time steps size δt and final time T.

	$\delta t=1/11$	$\delta t=1/12$	$\delta t=1/13$	$\delta t=1/14$	$\delta t=1/15$
$T=1$					
Maxerror	1.009E−01	9.472E−02	8.919E−02	8.426E−02	7.984E−02
RMSE	1.063E−02	9.704E−03	8.921E−03	8.253E−03	7.677E−03
$T=2$					
Maxerror	9.775E−02	9.188E−02	8.666E−02	8.200E−02	9.958E−02
RMSE	7.338E−03	6.709E−03	6.178E−03	5.724E−03	5.736E−03
$T=3$					
Maxerror	9.672E−02	9.098E−02	8.585E−02	8.138E−02	2.740E+02
RMSE	5.943E−03	5.438E−03	5.011E−03	4.644E−03	1.414E+01

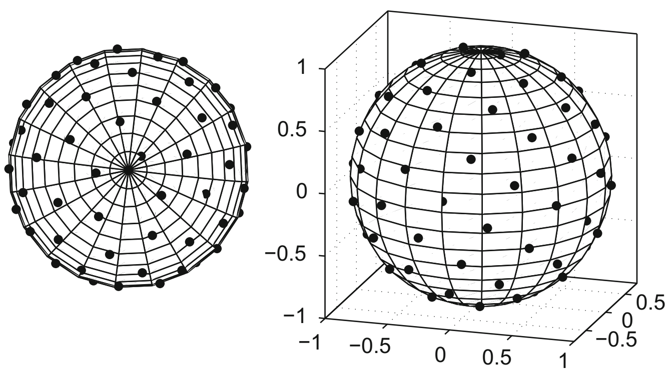

Fig. 8. The domain with uniform boundary collocation points.

Table 5
Maxerror and RMSE with different time step size δt and final time T.

	$\delta t=1$	$\delta t=1/2$	$\delta t=1/3$	$\delta t=1/4$	$\delta t=1/5$
$T=1$					
Maxerror	8.042E−04	6.064E−04	6.314E−04	6.894E−04	7.871E−04
RMSE	2.082E−04	1.319E−04	1.235E−04	1.247E−04	1.282E−04
$T=2$					
Maxerror	8.001E−04	6.378E−04	6.350E−04	7.102E−04	8.024E−05
RMSE	1.743E−04	1.085E−04	9.848E−05	9.800E−05	9.954E−05
$T=5$					
Maxerror	8.294E−04	6.040E−04	6.302E−04	7.108E−04	7.707E−04
RMSE	2.019E−04	1.172E−04	1.045E−04	1.037E−04	1.050E−04

Example 4. Consider the following nonhomogeneous heat conduction equation

$$\frac{\partial}{\partial t}u(\mathbf{x},t)+f(\mathbf{x},t)=\Delta u(\mathbf{x},t), \quad (\mathbf{x},t)\in\Omega\times(0,T)\subset\mathbb{R}^3\times\mathbb{R}^+, \quad \mathbf{x}=(x,y,z), \tag{35}$$

with final condition

$$u(\mathbf{x},T)=\sin(x)\sin(y)\sin(z)\cos(T), \quad \mathbf{x}\in\Omega, \tag{36}$$

and measured Dirichlet boundary condition

$$u(\mathbf{x},t)=\sin(x)\sin(y)\sin(z)\cos(t), \quad \mathbf{x}\in\partial\Omega, \ t>0, \tag{37}$$

where

$$f(\mathbf{x},t)=\sin(x)\sin(y)\sin(z)(\sin(t)-3\cos(t))$$

and the analytical solution given by:

$$u(\mathbf{x},t)=\sin(x)\sin(y)\sin(z)\cos(t). \tag{38}$$

The domain Ω is the sphere defined by:

$$\Omega=\{(x,y,z): x^2+y^2+z^2\le 1\} \tag{39}$$

as shown in Fig. 8.

In the computation, we choose $n_I=485$, $n_B=40$, $\delta=10^{-4}$, $c=1$ and $N=485$. It can be seen that the proposed method produces an accurate numerical solution where the Maxerror and RMSE are shown in Table 5 using various time step sizes $\delta t=1,1/2,1/3,1/4,1/5$.

4. Conclusion

Based on the idea of radial basis functions approximation and the method of particular solutions, we develop in this paper a new meshless computational method to solve nonhomogeneous backward heat conduction problems. Numerical examples are given in both two- and three-dimensional spatial spaces to indicate the efficiency and accuracy of the proposed method. For illustration purpose, we simply use the multiquadric basis function with constant shape parameter for all the numerical computations. Better numerical approximation to the solution is expected from using some recent works on deriving an optimal shape parameter. Finally, the proposed method is truly meshless and hence can be extended to solve problems in higher dimension under complicated and irregular domains.

Acknowledgements

The work described in this paper was partially supported by a grant from the Research Grants Council of the Hong Kong Special Administrative Region, China (Project no. CityU 101209) and was also supported by the National Natural Science Foundation of China (10671086) and the Shandong Natural Science Foundation.

References

[2] Chang JR, Liu CS, Chang CW. A new shooting method for quasi-boundary regularization of backward heat conduction problems. International Journal of Heat and Mass Transfer 2007;50:2325–32.
[3] Chen LY, Chen JT, Hong HK, Chen CH. Application of cesaro mean and the L-curve for the deconvolution problem. Soil Dynamics and Earthquake Engineering 1995;14:361–73.
[4] Cheng AHD, Cabral JJSP. Direct solution of ill-posed boundary value problems by radial basis function collocation method. International Journal for Numerical Methods in Engineering 2005;64(1):45–64.
[7] Feng XL, Qian Z, Fu CL. Numerical approximation of solution of nonhomogeneous backward heat conduction problem in bounded region. Mathematics and Computers in Simulation 2008;79:177–88.
[8] Fredman TP. A boundary identification method for an inverse heat conduction problem with an application in ironmaking. International Journal of Heat and Mass Transfer 2004;41:95–103.
[10] Hadamard J. Lectures on Cauchy problems in linear partial differential equations. New Haven, CT: Yale University Press; 1923.
[11] Han H, Ingham DB, Yuan Y. The boundary element method for the solution of the back ward heat conduction equation. Journal of Computational Physics 1995;116:292–9.
[13] Hansen PC. Analysis of discrete ill-posed problems by means of the L-curve. SIAM Review 1992;34:561–80.
[14] Hansen PC. Numerical tools for analysis and solution of Fredholm integral equations of the first kind. Inverse Problems 1992;8:849–72.
[15] Hansen PC. The L-curve and its use in the numerical treatment of inverse problems. In: Johnston P, editor. Computational inverse problems in electrocardiology, advances in computational bioengineering series, vol. 4. Southampton: WIT Press; 2000. p. 119–42.
[16] Hansen PC. Regularization tools: a Matlab package for analysis and solution of discrete ill-posed problems. Numerical Algorithms 1994;6:1–35.
[17] Hansen PC, O'Leary DP. The use of the L-curve in the regularization of discrete ill-posed problems. SIAM Journal on Scientific Computing 1993;14:1487–503.
[18] Hào DN. A mollification method for ill-posed problem. Numerische Mathematik 1994;68:469–506.

[19] Hon YC, Li M. A discrepancy principle for the source points location in using the MFS for solving the BHCP. International Journal of Computational Methods 2008;6(2):181–97.
[20] Hon YC, Wei T. A fundamental solution method for inverse heat conduction problem. Engineering Analysis with Boundary Elements 2004;28:489–95.
[21] Hon YC, Wei T. Numerical computation for multidimensional inverse heat conduction problem. Computer Modeling in Engineering & Sciences 2005;7(2):119–32.
[22] Huang CS, Lee CF, Cheng AHD. Error estimate, optimal shape factor, and high precision computation of multiquadric collocation method. Engineering Analysis with Boundary Elements 2007;31(7):614–23.
[24] Jourhmane M, Mera NS. An iterative algorithm for the backward heat conduction problem based on variable relaxation factors. Inverse Problems in Engineering 2002;10:293–308.
[25] Lattes R, Lions JL. The method of quasi-reversibility. New York: American Elsevier Publisher; 1969.
[26] Lawson CL, Hanson RJ. Solving least squares problems. Englewood Cliffs: Prentice-Hall Inc.; 1974.
[27] Lesnic D, Elliott L, Ingham DB. An iterative boundary element method for solving the back ward heat conduction problem using an elliptic approximation. Inverse Problems in Engineering 1998;6:255–79.
[28] Lijima K. Numerical solution of backward heat conduction problems by a high order lattice-free finite difference method. Journal of the Chinese Institute of Engineers 2004;27(4):611–20.
[29] Mera NS. The method of fundamental solutions for the backward heat conduction problem. Inverse Problems in Science and Engineering 2005;13(1):65–78.
[30] Miranker WL. A well posed problem for the backward heat equation. Proceedings of the American Mathematical Society 1961;12:243–7.
[31] Payne LE. Improperly posed problems in partial differential equations. Philadelphia: Society for Industrial and Applied Mathematics; 1975.
[32] Shidfar A, Zakeri A. A numerical technique for backward inverse heat conduction problems in one-dimensional space. Applied Mathematics and Computation 2005;171(2):1016–24.
[33] Tautenhahn U, Hämarik U. The use of monotonicity for choosing the regularization parameter in ill-posed problems. Inverse Problems 1999;15:1487–505.
[34] Tikhonov AN, Arsenin VY. The Solution of Ill-posed problems. New York: John Wiley and Sons; 1977.
[35] Zhou DY, Wei T. The method of fundamental solutions for solving a Cauchy problem of Laplace's equation in a multi-connected domain. Inverse Problems in Science and Engineering 2008;16(3):389–411.